

Topological flat bands in optical checkerboard-like lattices

Tomi Paananen and Thomas Dahm¹

¹*Universität Bielefeld, Fakultät für Physik, Postfach 100131, D-33501 Bielefeld, Germany*

(Dated: August 13, 2022)

We present comparatively simple two-dimensional and three-dimensional checkerboard-like optical lattices possessing nontrivial topological properties. By simple tuning of the parameters these lattices can have a topological insulating phase, a topological semi-metallic phase, or a trivial insulating phase. This allows study of different topological phase transitions within a single cold atom system. In the topologically nontrivial phases flat bands appear at the surfaces of the system. These surface states possess short localization lengths such that they are observable even in systems with small lattice dimensions. Our proposed lattices neither need spin-orbit coupling nor non-Abelian gauge fields to reach topologically nontrivial states.

PACS numbers: 67.85.-d, 37.10.Jk, 05.30.Fk, 03.65.Vf

I. INTRODUCTION

The theoretical prediction [1, 2] and experimental discovery of topological insulators [3, 4] has spurred the interest in nontrivial topological phases. The common property of these systems is the fact that surface states are protected by topological quantum numbers, making them particularly stable against different kinds of perturbations [5]. In particular, topological semi-metals like Dirac semi-metals and Weyl semi-metals and their unusual surface states have been studied recently in condensed-matter systems [6–11].

Optical lattices with cold atoms are perfect tools to simulate condensed matter problems. Using optical lattices one can modify lattice depths and lattice structures [12–15]. That is why almost any condensed matter system can be simulated using optical lattices. Interactions between cold atoms can also be tuned via the Feshbach resonance [16]. Several proposals have been made to realize topologically nontrivial states in cold atom systems [17–23] and recently a first experimental realization in a one-dimensional optical lattice was demonstrated [24]. Experimental detection of surface states is possible by Bragg spectroscopy [18, 20].

In the present work we make a specific proposal, how topological surface flat bands can be realized using comparatively simple optical lattices. Surface flat band states are particularly interesting, because the group velocity vanishes, and highly localized states can be formed. Also, the effect of interactions becomes particularly important in flat bands allowing new states of quantum matter [25, 26]. Topological flat bands have been found previously in other condensed matter systems like graphene, superfluid ³He, or unconventional superconductors [27–43] and may also appear in topological insulators with a time-reversal breaking ferromagnetic exchange field [44, 45]. The appearance of flat bands in *d*-wave superconductors as surface Andreev bound states has been studied intensively in the past both theoretically and experimentally [35–37, 46–57]. It has been suggested recently that the combination of superfluidity with flat bands can lead to very high critical temperatures [58, 59] for surface superconductivity. Using optical lattices with ultra-cold atoms such surface flat bands and in particular the influence of interactions on them could be studied in a very controlled way.

In this work, we will present a two dimensional (2D) and a three dimensional (3D) optical lattice model, possessing one dimensional and two dimensional surface flat bands, respectively. We will give simple analytical criteria for existence and location of these flat bands. We demonstrate that the system can be tuned from a topological insulating phase via a topological semi-metallic phase to a trivial insulating phase by tuning the intensity of the lasers creating the lattice. This allows study of various interesting topological phase transitions within a single model. We also show that in the 3D case the flat bands are always two dimensional, and the flat bands can be doubly degenerate under some circumstances. Flat bands can appear both for an insulating as well as a semi-metallic bulk phase. The appearance of the flat bands can be understood in terms of a classification recently proposed by Matsuura et al [60] using a topological invariant in the presence of a chiral symmetry.

II. MODELS

A. Two-dimensional model

Our model is a tight binding checkerboard model with different forward and backward hoppings. The Hamiltonian can be written as

$$\hat{H}_{2D} = \sum_{m,n} \left[-J_{1,x} \hat{a}_{1,m,n}^\dagger \hat{b}_{1,m,n} - J_{2,x} \hat{a}_{1,m,n}^\dagger \hat{b}_{1,m-1,n} - J_{1,x} \hat{a}_{2,m,n}^\dagger \hat{b}_{2,m+1,n} - J_{2,x} \hat{a}_{2,m,n}^\dagger \hat{b}_{2,m,n} \right. \\ \left. - J_{1,y} \hat{a}_{1,m,n}^\dagger \hat{b}_{2,m,n} - J_{2,y} \hat{a}_{1,m,n}^\dagger \hat{b}_{2,m,n-1} - J_{1,y} \hat{a}_{2,m,n}^\dagger \hat{b}_{1,m,n+1} - J_{2,y} \hat{a}_{2,m,n}^\dagger \hat{b}_{1,m,n} + h.c. \right], \quad (1)$$

where m and n are the unit cell indices, and \hat{a} and \hat{b} are annihilation operators for different sublattice sites. This Hamiltonian is essentially a two-dimensional generalization of the dimerized optical lattice that has been studied in Ref. 24. It consists of four sublattice sites per unit cell, as shown in Fig. 1. If the periodicity of the lattice is d , the lattice spacing of the sublattice is $d/2$. We can assume without loss of generality that $J_{1,\alpha} \geq J_{2,\alpha}$ (if this is not the case we can always relabel the hopping strengths and the sublattice sites). In Appendix A we discuss how such an optical lattice can be created by a certain laser arrangement. Recently there has been intensive experimental effort to create either spin-orbit coupling [22] or non-Abelian gauge potentials [61, 62] in cold atom systems in a desire to reach topologically nontrivial states. We note, that neither spin-orbit coupling nor a non-Abelian gauge potential is needed to create the present lattice. Nevertheless, nontrivial topology appears for certain parameter ranges, as shown below.

If one takes the Fourier transform of the Hamiltonian, it can be written as

$$H_{2D} = \sum_{\mathbf{k}} \hat{\Psi}_{\mathbf{k}}^\dagger \begin{pmatrix} 0 & 0 & f_x^*(k_x) & f_y^*(k_y) \\ 0 & 0 & f_y^*(k_y) & f_x^*(k_x) \\ f_x(k_x) & f_y(k_y) & 0 & 0 \\ f_y(k_y) & f_x(k_x) & 0 & 0 \end{pmatrix} \hat{\Psi}_{\mathbf{k}}, \quad (2)$$

where $\mathbf{k} = (k_x, k_y)$,

$$\hat{\Psi}_{\mathbf{k}} = (\hat{a}_{1,\mathbf{k}}, \hat{a}_{2,\mathbf{k}}, \hat{b}_{1,\mathbf{k}}, \hat{b}_{2,\mathbf{k}})^T,$$

and

$$f_\alpha(k_\alpha) = -J_{1,\alpha} e^{ik_\alpha d/2} - J_{2,\alpha} e^{-ik_\alpha d/2}. \quad (3)$$

The Hamiltonian possesses particle-hole symmetry, if the system is half-filled with two fermions per unit cell. Also, time-reversal symmetry, parity symmetry, and most importantly a chiral symmetry

$$S = \begin{pmatrix} 1 & 0 & 0 & 0 \\ 0 & 1 & 0 & 0 \\ 0 & 0 & -1 & 0 \\ 0 & 0 & 0 & -1 \end{pmatrix} \quad (4)$$

is respected, i.e. H_{2D} and S anticommute. As has been discussed in Ref. 63, 64, the chiral symmetry S is essential for the existence of edge flat bands. Note that the phases of f_x and f_y are Berry's phases and cannot be transformed away.

The single particle Hamiltonian has an off-diagonal block form, thus the methods from Ref. 60, 65 can be used to treat the Hamiltonian. In our case the block is given by

$$D_{2D}(\mathbf{k}) = \begin{pmatrix} f_x(k_x) & f_y(k_y) \\ f_y(k_y) & f_x(k_x) \end{pmatrix} \quad (5)$$

For a boundary perpendicular to the x -direction, the existence of edge flat bands is connected to the value of the following winding number [60, 65]

$$w(k_y) = \frac{1}{2\pi} \text{Im} \left(\int_{-\pi}^{\pi} dk_x \frac{\partial_{k_x} \text{Det}(D_{2D}(\mathbf{k}))}{\text{Det}(D_{2D}(\mathbf{k}))} \right). \quad (6)$$

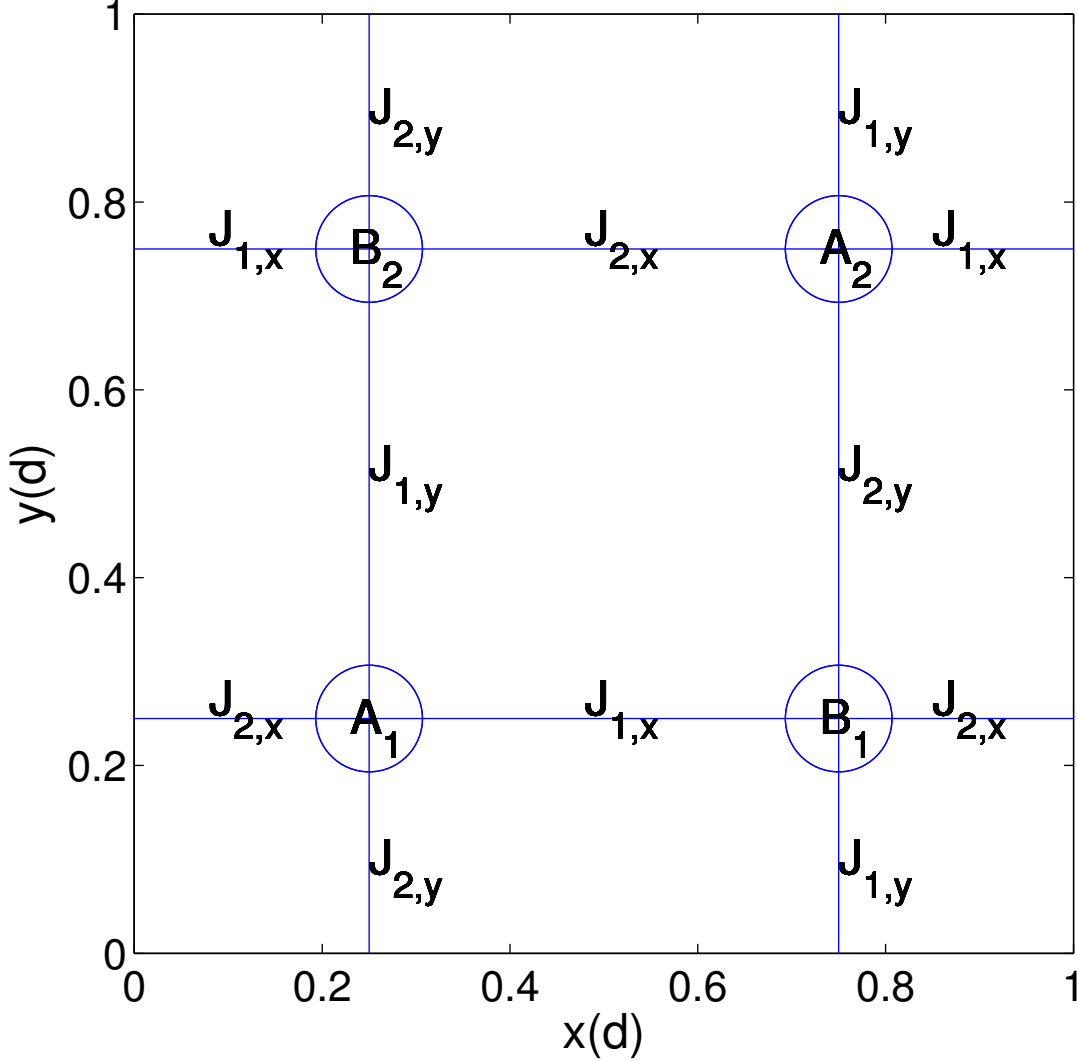


FIG. 1: Schematic figure of the sublattice structure and the corresponding hopping strengths.

Here we have set $d = 1$. We can define the path $\gamma(k_x) = \text{Det}(D_{2D}(\mathbf{k})) = f_x(k_x)^2 - f_y(k_y)^2$ in the complex plane. Then, this integral can be written as a path integral as follows

$$w(k_y) = \frac{1}{2\pi i} \oint_{\gamma} \frac{dz}{z}. \quad (7)$$

This shows that the winding number $w(k_y)$ is always an integer. If it equals to zero we do not have a flat band at the surface, otherwise we have. However, this formula is not very useful to determine the values of k_y for which a flat band exists. Instead, setting $z = e^{ik_x d}$ integral (6) can be mapped to a path integral over the unit circle, and the integrand is then given by

$$f_{2D}(z) = \frac{J_{1,x}^2 z^2 - J_{2,x}^2}{z[(J_{1,x}z + J_{2,x})^2 - z f_y(k_y)^2]} = \frac{-1}{z} + \frac{1}{z - w_+} + \frac{1}{z - w_-}, \quad (8)$$

where

$$w_{\pm} = \left(\frac{f_y(k_y) \pm \sqrt{f_y(k_y)^2 - 4J_{1,x}J_{2,x}}}{2J_{1,x}} \right)^2. \quad (9)$$

Let us assume first that $J_{1,x} > J_{2,x}$. The absolute values of w_{\pm} determine whether we have a flat band or not. It is easy to prove that one of the absolute values is always smaller than $J_{2,x}/J_{1,x} < 1$. Thus, if both are smaller than 1 we have a flat band, if not we do not have a flat band. It turns out that

$$\begin{aligned} \max(|w_+|, |w_-|) &\leq \left(\frac{(J_{1,x} - J_{2,x})|V_{k_y}| + \sqrt{[(J_{1,x} - J_{2,x})|V_{k_y}|]^2 + 4J_{1,x}J_{2,x}}}{2J_{1,x}} \right)^2, \text{ if } |V_{k_y}| < 1 \\ \max(|w_+|, |w_-|) &= 1, \text{ if } |V_{k_y}| = 1 \\ \max(|w_+|, |w_-|) &\geq \left(\frac{(J_{1,x} - J_{2,x})|V_{k_y}| + \sqrt{[(J_{1,x} - J_{2,x})|V_{k_y}|]^2 + 4J_{1,x}J_{2,x}}}{2J_{1,x}} \right)^2, \text{ if } |V_{k_y}| > 1, \end{aligned} \quad (10)$$

where

$$|V_{k_y}|^2 = \left(\frac{J_{1,y} + J_{2,y}}{J_{1,x} + J_{2,x}} \right)^2 \cos^2(k_y/2) + \left(\frac{J_{1,y} - J_{2,y}}{J_{1,x} - J_{2,x}} \right)^2 \sin^2(k_y/2) = a_y^2 \cos^2(k_y/2) + b_y^2 \sin^2(k_y/2)$$

with $a_y = \left| \frac{J_{1,y} + J_{2,y}}{J_{1,x} + J_{2,x}} \right|$ and $b_y = \left| \frac{J_{1,y} - J_{2,y}}{J_{1,x} - J_{2,x}} \right|$. Equation (10) shows that $\max(|w_+|, |w_-|) < 1$, if $|V_{k_y}| < 1$, and $\max(|w_+|, |w_-|) > 1$, if $|V_{k_y}| > 1$. From this we can deduce that we have a flat band only if $|V_{k_y}| < 1$. From equation (10) we can deduce the following: If both $a_y < 1$ and $b_y < 1$, we have an edge flat band for all k_y , and the bulk is an insulator. Thus in this case the flat bands are isolated. If $a_y \geq 1$ and $b_y < 1$, we have a flat band for

$$|k_y| > 2 \arccos \left(\sqrt{\frac{1 - b_y^2}{a_y^2 - b_y^2}} \right),$$

and the bulk is a topological semi-metal. If $a_y < 1$ and $b_y \geq 1$, we have a flat band for

$$|k_y| < 2 \arccos \left(\sqrt{\frac{b_y^2 - 1}{b_y^2 - a_y^2}} \right),$$

with the bulk being a semi-metal, too. If both $a_y \geq 1$ and $b_y \geq 1$, we have no flat bands. If $a_y > 1$ and $b_y > 1$, we have an insulating bulk without edge states, i.e. a topologically trivial insulator. Thus, by tuning the optical lattice potential via the parameters a_y and b_y it becomes possible to drive the system into different topological phases.

In order to confirm these analytical results based on the winding number given in Ref. [60], we numerically determined all eigenvalues by exact diagonalization of Hamiltonian (1) on a finite lattice. We use periodical boundary conditions in y -direction and open boundary conditions in x -direction. Results of the numerical exact diagonalization on a 200×200 lattice are shown in figure 2, which presents the energy spectra as a function of momentum k_y parallel to the surface for $J_{1,x} = 1.0$ and $J_{2,x} = 0.5$ with different values of $J_{1,y}$ and $J_{2,y}$. Figure 2 (a) shows if $a_y < 1$ and $b_y < 1$, we have an edge flat band for all k_y , and the bulk is an insulator. Figure 2 (b) shows if $a_y > 1$ and $b_y < 1$, we have an edge flat band if

$$|k_y| > 2 \arccos \left(\sqrt{\frac{1 - b_y^2}{a_y^2 - b_y^2}} \right).$$

Figure 2 (c) shows if $a_y < 1$ and $b_y > 1$, we have an edge flat band if

$$|k_y| < 2 \arccos \left(\sqrt{\frac{b_y^2 - 1}{b_y^2 - a_y^2}} \right).$$

Finally, figure 2 (d) shows if $a_y > 1$ and $b_y > 1$, we only have an insulating bulk without flat bands.

In figure 3 we show the occupation probabilities $|\rho(n)|^2$ as a function of unit cell index n of selected edge (a-c) and bulk (d) states for $J_{1,x} = 1.0$ and $J_{2,x} = 0.5$ with different values of $J_{1,y}$ and $J_{2,y}$. We see from figures 3 (a-c) that the edge states are well localized on the boundary within the first 5 to 10 lattice sites. Thus the flat bands should be visible even for small lattice size. The localization becomes better, if $|J_{1,x} - J_{2,x}|/(J_{1,x} + J_{2,x})$ increases.

If $J_{2,x} = J_{1,x}$ we have no flat bands. In this case the method described above cannot always be used, because the integral (6) does not converge in this case. However, in this case we can deduce that, if $k_y \neq 0$ and $J_{y,1} \neq J_{y,2}$, $\max(|w_+|, |w_-|) > 1$ and $\min(|w_+|, |w_-|) < 1$. Thus no flat bands appear. If $k_y = 0$ or $J_{y,1} = J_{y,2}$, the integral (6) does not converge, because of poles on the integration path. In this case the projection of the Fermi surface onto the boundary forms a continuum with the bulk states, thus we have no edge flat bands.

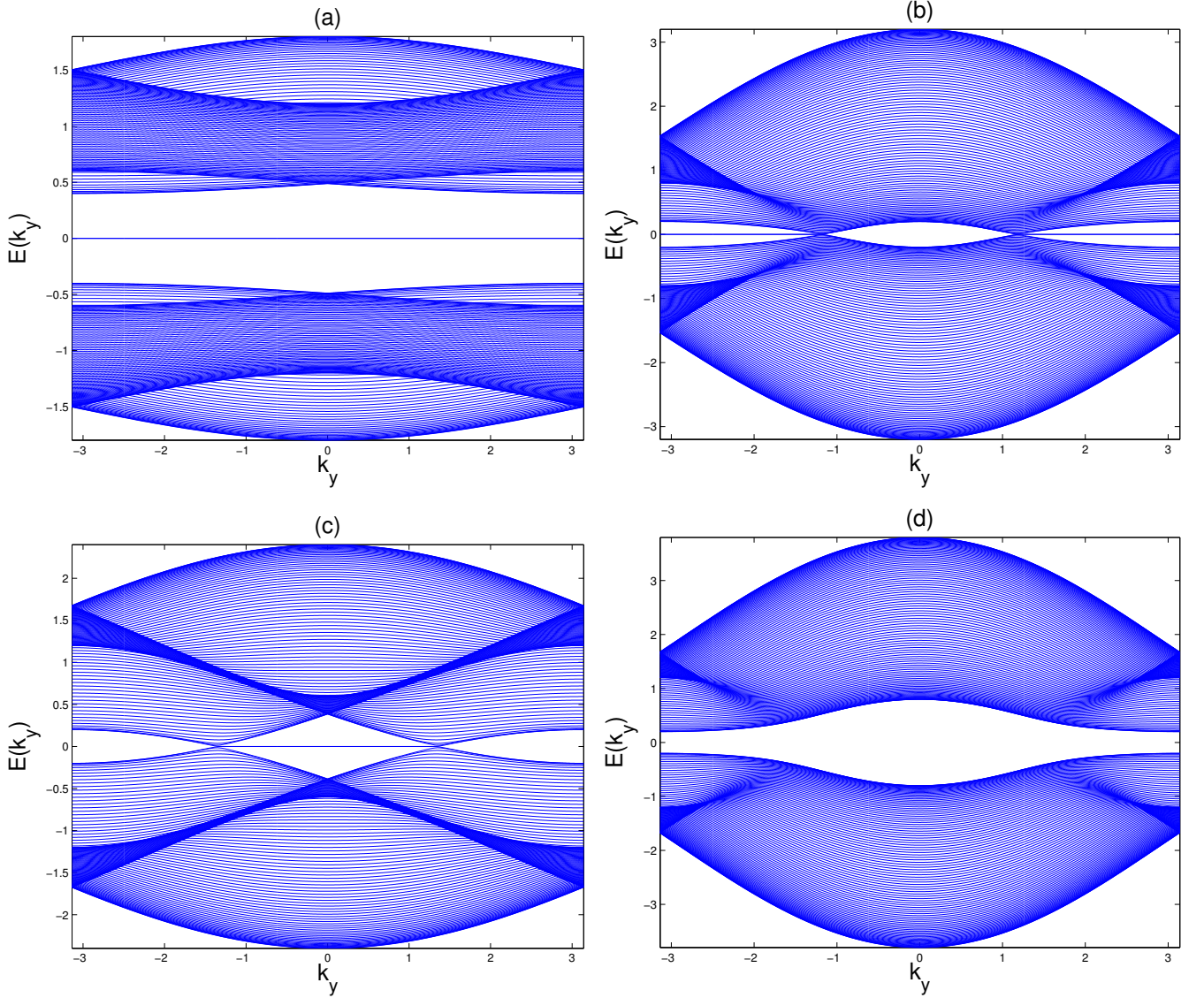


FIG. 2: Numerical 2D dispersions of bulk and edge states for $J_{1,x} = 1.0$ and $J_{2,x} = 0.5$ with different values of $J_{1,y}$ and $J_{2,y}$. In figure (a) $J_{1,y} = 0.2$ and $J_{2,y} = 0.1$, in figure (b) $J_{1,y} = 1.0$ and $J_{2,y} = 0.7$, in figure (c) $J_{1,y} = 0.8$ and $J_{2,y} = 0.1$, and in figure (d) $J_{1,y} = 1.5$ and $J_{2,y} = 0.8$.

B. Three-dimensional model

The three dimensional case is a direct generalization of the 2D case. The Hamiltonian can be written as

$$\begin{aligned}
 \hat{H}_{3D} = \sum_{m,n,i} \bigg[& -J_{1,x} \hat{a}_{1,m,n,i}^\dagger \hat{b}_{1,m,n,i} - J_{2,x} \hat{a}_{1,m,n,i}^\dagger \hat{b}_{1,m-1,n,i} - J_{1,x} \hat{a}_{2,m,n,i}^\dagger \hat{b}_{2,m+1,n,i} - J_{2,x} \hat{a}_{2,m,n,i}^\dagger \hat{b}_{2,m,n,i} \\
 & - J_{1,x} \hat{a}_{3,m,n,i}^\dagger \hat{b}_{3,m+1,n,i} - J_{2,x} \hat{a}_{3,m,n,i}^\dagger \hat{b}_{3,m,n,i} - J_{1,x} \hat{a}_{4,m,n,i}^\dagger \hat{b}_{4,m,n,i} - J_{2,x} \hat{a}_{4,m,n,i}^\dagger \hat{b}_{4,m-1,n,i} \\
 & - J_{1,y} \hat{a}_{1,m,n,i}^\dagger \hat{b}_{2,m,n,i} - J_{2,y} \hat{a}_{1,m,n,i}^\dagger \hat{b}_{2,m,n-1,i} - J_{1,y} \hat{a}_{2,m,n,i}^\dagger \hat{b}_{1,m,n+1,i} - J_{2,y} \hat{a}_{2,m,n,i}^\dagger \hat{b}_{1,m,n,i} \\
 & - J_{1,y} \hat{a}_{3,m,n,i}^\dagger \hat{b}_{4,m,n+1,i} - J_{2,y} \hat{a}_{3,m,n,i}^\dagger \hat{b}_{4,m,n,i} - J_{1,y} \hat{a}_{4,m,n,i}^\dagger \hat{b}_{3,m,n} - J_{2,y} \hat{a}_{4,m,n,i}^\dagger \hat{b}_{3,m,n-1,i} \\
 & - J_{1,z} \hat{a}_{1,m,n,i}^\dagger \hat{b}_{3,m,n,i} - J_{2,z} \hat{a}_{1,m,n,i}^\dagger \hat{b}_{3,m,n,i-1} - J_{1,z} \hat{a}_{2,m,n,i}^\dagger \hat{b}_{4,m,n,i} - J_{2,z} \hat{a}_{2,m,n,i}^\dagger \hat{b}_{4,m,n,i-1} \\
 & - J_{1,z} \hat{a}_{3,m,n,i}^\dagger \hat{b}_{2,m,n,i+1} - J_{2,z} \hat{a}_{3,m,n,i}^\dagger \hat{b}_{2,m,n,i} - J_{1,z} \hat{a}_{4,m,n,i}^\dagger \hat{b}_{1,m,n,i+1} - J_{2,z} \hat{a}_{4,m,n,i}^\dagger \hat{b}_{1,m,n,i} + h.c. \bigg], \tag{11}
 \end{aligned}$$

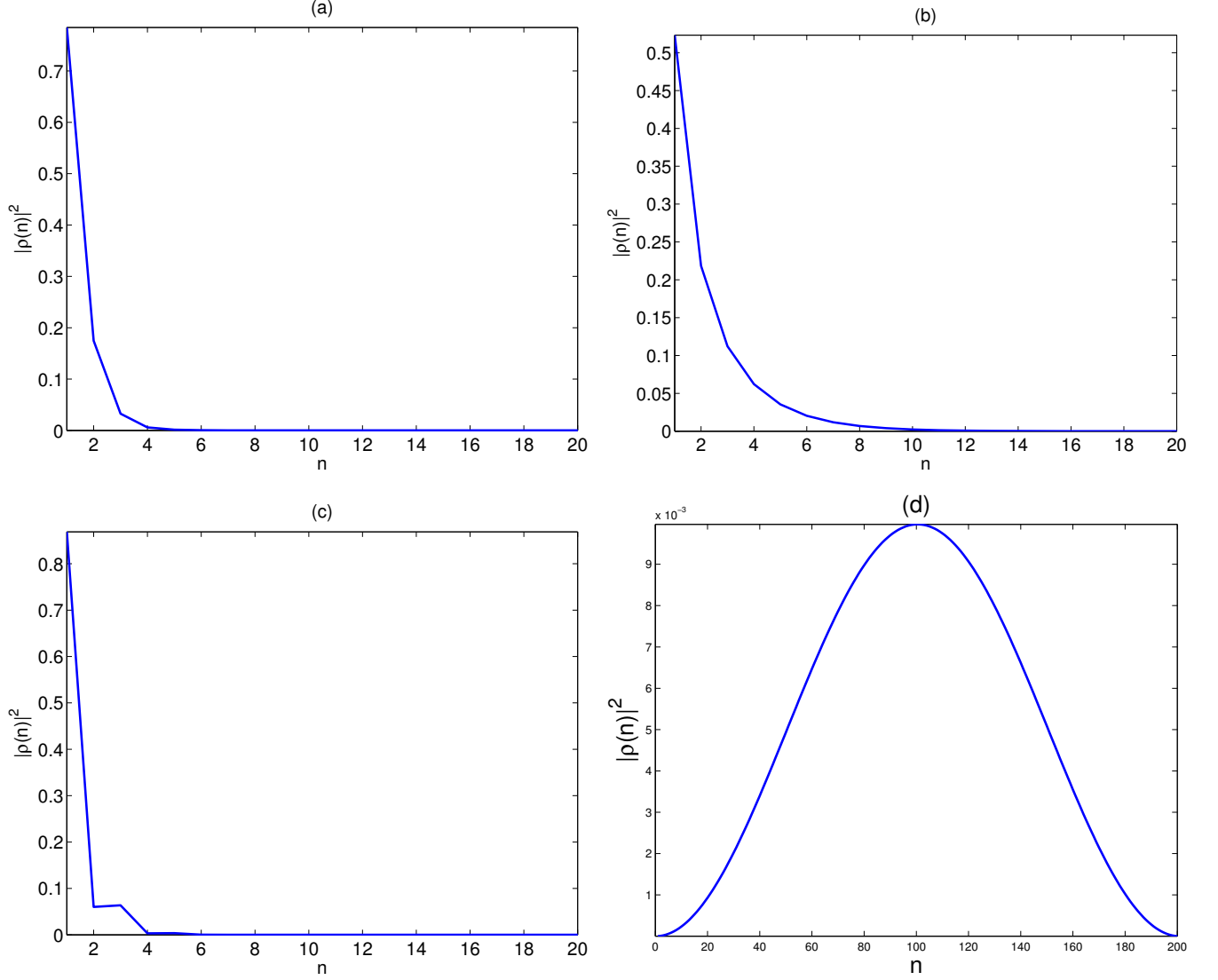


FIG. 3: Occupation probabilities $|\rho(n)|^2$ as a function of unit cell index n of selected edge (a-c) and bulk (d) states for $J_{1,x} = 1.0$ and $J_{2,x} = 0.5$ with different values of $J_{1,y}$ and $J_{2,y}$. In figure (a) $J_{1,y} = 0.2$, $J_{2,y} = 0.1$, and $k_y = 0$ in figure (b) $J_{1,y} = 1.0$, $J_{2,y} = 0.7$, and $k_y = \pi$, in figure (c) $J_{1,y} = 0.8$, $J_{2,y} = 0.1$, and $k_y = 0$, and in figure (c) $J_{1,y} = 1.5$, $J_{2,y} = 0.8$, and $k_y = 0$.

where m , n , and i are the unit cell indices, and \hat{a} and \hat{b} are annihilation operators. This Hamiltonian consists of eight sublattice sites per unit cell.

If one takes a Fourier transform of the Hamiltonian, the Hamiltonian can be written as

$$H_{3D} = \sum_{\mathbf{k}} \hat{\Psi}_{\mathbf{k}}^\dagger \begin{pmatrix} 0 & 0 & 0 & 0 & f_x^*(k_x) & f_y^*(k_y) & f_z^*(k_z) & 0 \\ 0 & 0 & 0 & 0 & f_y^*(k_y) & f_x^*(k_x) & 0 & f_z^*(k_z) \\ 0 & 0 & 0 & 0 & f_z^*(k_z) & 0 & f_x^*(k_x) & f_y^*(k_y) \\ 0 & 0 & 0 & 0 & 0 & f_z^*(k_z) & f_y^*(k_y) & f_x^*(k_x) \\ f_x(k_x) & f_y(k_y) & f_z(k_z) & 0 & 0 & 0 & 0 & 0 \\ f_y(k_y) & f_x(k_x) & 0 & f_z(k_z) & 0 & 0 & 0 & 0 \\ f_z(k_z) & 0 & f_x(k_x) & f_y(k_y) & 0 & 0 & 0 & 0 \\ 0 & f_z(k_z) & f_y(k_y) & f_x(k_x) & 0 & 0 & 0 & 0 \end{pmatrix} \hat{\Psi}_{\mathbf{k}}, \quad (12)$$

where $\mathbf{k} = (k_x, k_y, k_z)$,

$$\hat{\Psi}_{\mathbf{k}} = (\hat{a}_{1,\mathbf{k}}, \hat{a}_{2,\mathbf{k}}, \hat{a}_{3,\mathbf{k}}, \hat{a}_{4,\mathbf{k}}, \hat{b}_{1,\mathbf{k}}, \hat{b}_{2,\mathbf{k}}, \hat{b}_{3,\mathbf{k}}, \hat{b}_{4,\mathbf{k}})^T,$$

and

$$f_\alpha(k_\alpha) = -J_{1,\alpha}e^{ik_\alpha d/2} - J_{2,\alpha}e^{-ik_\alpha d/2}. \quad (13)$$

As in the 2D case this Hamiltonian has a particle-hole symmetry, time-reversal symmetry, and a parity symmetry. Most importantly the Hamiltonian exhibits a chiral symmetry, again, allowing for the existence of topological edge flat bands [63, 64]. Also this Hamiltonian has an off-diagonal block form, thus the methods from reference [60, 65] can be used to treat the Hamiltonian, again. In the present case the block is given by

$$D_{3D}(\mathbf{k}) = \begin{pmatrix} f_x(k_x) & f_y(k_y) & f_z(k_z) & 0 \\ f_y(k_y) & f_x(k_x) & 0 & f_z(k_z) \\ f_z(k_z) & 0 & f_x(k_x) & f_y(k_y) \\ 0 & f_z(k_z) & f_y(k_y) & f_x(k_x) \end{pmatrix}. \quad (14)$$

If we consider a boundary perpendicular to the x -direction, the existence of edge flat bands is connected to the value of the following winding number [60, 65]

$$w(k_y, k_z) = \frac{1}{2\pi} \text{Im} \left(\int_{-\pi}^{\pi} dk_x \frac{\partial_{k_x} \text{Det}(D_{3D}(\mathbf{k}))}{\text{Det}(D_{3D}(\mathbf{k}))} \right). \quad (15)$$

Again, this integral can be mapped to a path integral over the unit circle, and the integrand is then given by

$$f_{3D}(z) = \frac{p_1(z)}{z p_2(z)}, \quad (16)$$

where

$$\begin{aligned} p_1(z) &= 2J_{1,x}^4 z^4 + 4J_{1,x}^3 J_{2,x} z^3 - 4J_{2,x}^3 J_{1,x} z - 2J_{2,x}^4 - 2(J_{1,x}^2 z^3 - J_{2,x}^2 z)(f_y(k_y)^2 + f_z(k_z)^2), \\ p_2(z) &= (J_{1,x} z + J_{2,x})^4 - 2z[(J_{1,x} z + J_{2,x})^2(f_y(k_y)^2 + f_z(k_z)^2)] + z^2[f_y(k_y)^4 + f_z(k_z)^4 - 2f_y(k_y)^2 f_z(k_z)^2]. \end{aligned}$$

Integrand (16) can be simplified as

$$f_{3D}(z) = \frac{-2}{z} + \frac{1}{z - w_+^+} + \frac{1}{z - w_-^+} + \frac{1}{z - w_+^-} + \frac{1}{z - w_-^-}, \quad (17)$$

where

$$\begin{aligned} w_\pm^+ &= \left(\frac{(f_y(k_y) + f_z(k_z)) \pm \sqrt{(f_y(k_y) + f_z(k_z))^2 - 4J_{1,x}J_{2,x}}}{2J_{1,x}} \right)^2, \\ w_\pm^- &= \left(\frac{(f_y(k_y) - f_z(k_z)) \pm \sqrt{(f_y(k_y) - f_z(k_z))^2 - 4J_{1,x}J_{2,x}}}{2J_{1,x}} \right)^2. \end{aligned} \quad (18)$$

Thus the integral can assume the values $-2, -1, 0, 1, 2$. If the value is 0 there are no flat bands, but otherwise there are. If the value equals 2 (or -2) we find two degenerate flat bands.

Let us assume $J_{1,x} > J_{2,x}$. Now $\min(|w_+^+|, |w_-^+|) \leq J_{2,x}/J_{1,x} < 1$ and $\min(|w_+^-|, |w_-^-|) \leq J_{2,x}/J_{1,x} < 1$. Thus we have always at least two poles within the unit disc. Thus the value of the integral depends on the values of $\max(|w_+^+|, |w_-^+|)$ and $\max(|w_+^-|, |w_-^-|)$. It turns out that

$$\begin{aligned} \max(|w_+^\pm|, |w_-^\pm|) &\leq \left(\frac{(J_{1,x} - J_{2,x})|V_{k_y, k_z}^\pm| + \sqrt{[(J_{1,x} - J_{2,x})|V_{k_y, k_z}^\pm|]^2 + 4J_{1,x}J_{2,x}}}{2J_{1,x}} \right)^2, \text{ if } |V_{k_y, k_z}^\pm| < 1 \\ \max(|w_+^\pm|, |w_-^\pm|) &= 1, \text{ if } |V_{k_y, k_z}^\pm| = 1 \\ \max(|w_+^\pm|, |w_-^\pm|) &\geq \left(\frac{(J_{1,x} - J_{2,x})|V_{k_y, k_z}^\pm| + \sqrt{[(J_{1,x} - J_{2,x})|V_{k_y, k_z}^\pm|]^2 + 4J_{1,x}J_{2,x}}}{2J_{1,x}} \right)^2, \text{ if } |V_{k_y, k_z}^\pm| > 1, \end{aligned} \quad (19)$$

where

$$|V_{k_y, k_z}^\pm|^2 = \left(\frac{J_{1,y} + J_{2,y}}{J_{1,x} + J_{2,x}} \cos(k_y/2) \pm \frac{J_{1,z} + J_{2,z}}{J_{1,x} + J_{2,x}} \cos(k_z/2) \right)^2 + \left(\frac{J_{1,y} - J_{2,y}}{J_{1,x} - J_{2,x}} \sin(k_y/2) \pm \frac{J_{1,z} - J_{2,z}}{J_{1,x} - J_{2,x}} \sin(k_z/2) \right)^2$$

$$= (a_y \cos(k_y/2) \pm a_z \cos(k_z/2))^2 + (b_y \sin(k_y/2) \pm b_z \sin(k_z/2))^2.$$

If $|V_{k_y, k_z}^\pm| < 1$, $\max(|w_+^\pm|, |w_-^\pm|) < 1$, and if $|V_{k_y, k_z}^\pm| > 1$, $\max(|w_+^\pm|, |w_-^\pm|) > 1$. If both $\max(|w_+^\pm|, |w_-^\pm|)$ are smaller than 1 we find two flat bands, if only one is smaller than 1 we find a single flat band, if both are larger than 1 we find no flat bands.

The location (in the projected momentum space, i.e. in the $k_y k_z$ -plane) of the flat bands depends on the parameters a_y, a_z, b_y, b_z . Without loss of generality we can assume all these parameters non-negative. In this case $\sup_{k_y, k_z} |V_{k_y, k_z}^+| \geq \sup_{k_y, k_z} |V_{k_y, k_z}^-|$ and $\inf_{k_y, k_z} |V_{k_y, k_z}^+| \geq \inf_{k_y, k_z} |V_{k_y, k_z}^-|$. The values of $\sup_{k_y, k_z} |V_{k_y, k_z}^+|$, $\sup_{k_y, k_z} |V_{k_y, k_z}^-|$, $\inf_{k_y, k_z} |V_{k_y, k_z}^+|$, and $\inf_{k_y, k_z} |V_{k_y, k_z}^-|$ can be found in Appendix B.

We have several different phase possibilities: (I) if $\sup_{k_y, k_z} |V_{k_y, k_z}^+| < 1$, the bulk is an insulator, and we find two isolated flat bands for every $\tilde{\mathbf{k}} = (k_y, k_z)$. (II) If $\sup_{k_y, k_z} |V_{k_y, k_z}^-| < 1$, $\sup_{k_y, k_z} |V_{k_y, k_z}^+| \geq 1$, and $\inf_{k_y, k_z} |V_{k_y, k_z}^+| < 1$, the bulk is a semimetal we find a flat band for all $\tilde{\mathbf{k}}$. For some $\tilde{\mathbf{k}}$ there are two flat bands, and one flat band for the rest. (III) If $\inf_{k_y, k_z} |V_{k_y, k_z}^+| < 1$ and $\sup_{k_y, k_z} |V_{k_y, k_z}^-| \geq 1$, the bulk is a semimetal. Flat bands can be found only in some part of the projected k -space. (IV) If $\inf_{k_y, k_z} |V_{k_y, k_z}^+| > 1$, $\inf_{k_y, k_z} |V_{k_y, k_z}^-| < 1$, and $\sup_{k_y, k_z} |V_{k_y, k_z}^-| \geq 1$, the bulk is a semimetal, and we have a non-degenerate flat band in some part of the projected momentum space. (V) If $\inf_{k_y, k_z} |V_{k_y, k_z}^-| > 1$, the bulk is an insulator, and we find no flat bands.

One could move from one phase to another by tuning the laser intensity.

Figure 4 shows some examples of 2D flat bands in the surface Brillouin zone for the different phases. In figure 4 (a) we show phase I with $J_{1,y} = J_{1,z} = 0.2$ and $J_{2,y} = J_{2,z} = 0.1$, here we see that the two-fold degenerate flat band totally fills the projected momentum space. Figure 4 (b) shows phase II with $J_{1,y} = 0.6$, $J_{1,z} = 0.4$, and $J_{2,y} = J_{2,z} = 0.2$, the two-fold degenerate flat band fills the projected momentum space only partially, and the rest of the momentum space (near the origin) is filled by a non-degenerate flat band. Phase III with $J_{1,y} = J_{1,z} = 1.0$, $J_{2,y} = 0.8$, and $J_{2,z} = 0.6$ is shown in figure 4 (c). In this case we see that only a part of the projected momentum space is occupied by the flat bands (degenerate and non-degenerate). In figure 4 (d) we show phase IV with $J_{1,y} = 2.0$, $J_{1,z} = 1.2$, $J_{2,y} = 0.3$, and $J_{2,z} = 0.4$. Here we see that only a non-degenerate flat band partially fills the projected momentum space. Throughout figure 4 we have set $J_{1,x} = 1.0$ and $J_{1,x} = 0.2$.

If $J_{1,x} = J_{2,x}$ there are no flat bands. The reasons are the same as in the 2D-case. If one looks at all three possible boundaries (perpendicular to x -, y -, or z -direction), the only situation when one cannot find any flat bands is the case, where $J_{1,x} = J_{2,x}$, $J_{1,y} = J_{2,y}$, and $J_{1,z} = J_{2,z}$. In this case the bulk is a metal (a standard cubic lattice). Thus if the bulk is an insulator or a semimetal one can always find flat bands at least at one of the boundaries.

III. CONCLUSION

We have presented both 2D and 3D optical lattices, which possess topological surface flat bands. These lattices can be relatively easy created by counterpropagating laser beams and do not require spin-orbit coupling nor non-Abelian gauge fields. By tuning the intensity of the potential it is possible to sweep between topological insulating, semi-metallic, and trivial insulating phases.

We derived simple analytical formulas for the existence and the location of the flat bands. We showed that in the 3D case we can have a double degeneracy of the flat bands. Also in the 3D case the flat bands are two dimensional, in contrast to other surface flat band systems, where the flat bands are one dimensional. Due to their short localization length, these flat bands could be realized in experiments even with a small lattice size.

These systems can be used to study the influence of interaction on the flat bands via a Feshbach resonance or to study high- T_c surface superfluidity. Also these systems can be used to model different flat bands systems with little modification.

Appendix A: Creation of the lattices

The corresponding 2D lattice can be formed using the following periodical potential

$$V_{2D}(x, y) = V_1 \cos^2\left(\frac{2\pi x}{d}\right) + V_2 \cos^2\left(\frac{2\pi y}{d}\right) + V_3 \cos^2\left(\frac{\pi(x+y)}{d} + \theta_1\right) + V_4 \cos^2\left(\frac{\pi(x-y)}{d} + \theta_2\right). \quad (\text{A1})$$

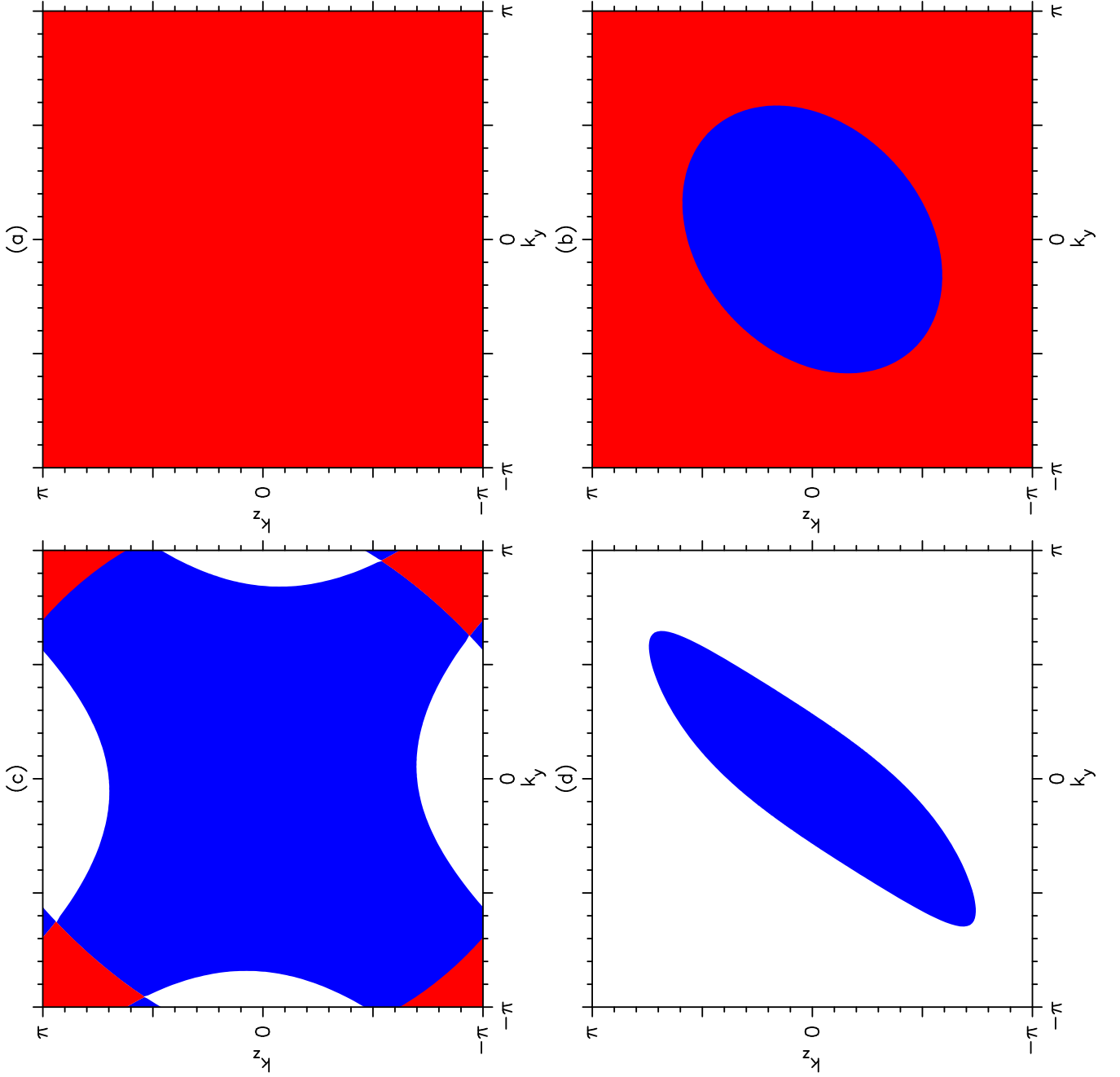


FIG. 4: Examples of 2D flat bands with different phases in the 3D case. Red: a two-fold degenerate zero energy flat band. Blue: a non-degenerate zero energy flat band. White: no flat bands. Figure (a) phase 1 $J_{1,y} = J_{1,z} = 0.2$ and $J_{2,y} = J_{2,z} = 0.1$. Figure (b) phase 2 $J_{1,y} = 0.6$, $J_{1,z} = 0.4$, and $J_{2,y} = J_{2,z} = 0.2$. Figure (c) phase 3 $J_{1,y} = J_{1,z} = 1.0$, $J_{2,y} = 0.8$, and $J_{2,z} = 0.6$. Figure (d) phase 4 $J_{1,y} = 2.0$, $J_{1,z} = 1.2$, $J_{2,y} = 0.3$, and $J_{2,z} = 0.4$. In all these figures $J_{1,x} = 1.0$ and $J_{2,x} = 0.2$.

To create this potential we need four lasers with wavelength $\lambda = d$ and four lasers with wavelength $2\lambda = 2d$, where d is the periodicity of the lattice. Figure 5 shows the laser arrangement schematically. Figure 6 shows an example of the 2D lattice potential. We can see from the figure that the barriers between the sublattice sites are different in the forward direction (alongside the axis) than in backward direction. This means that also the hopping strengths are different.

The three dimensional lattice is generalization of the 2D case. There are several ways to construct the three dimensional potential. For the following potential one needs 14 lasers, six with wavelegh λ and eight with 2λ . The

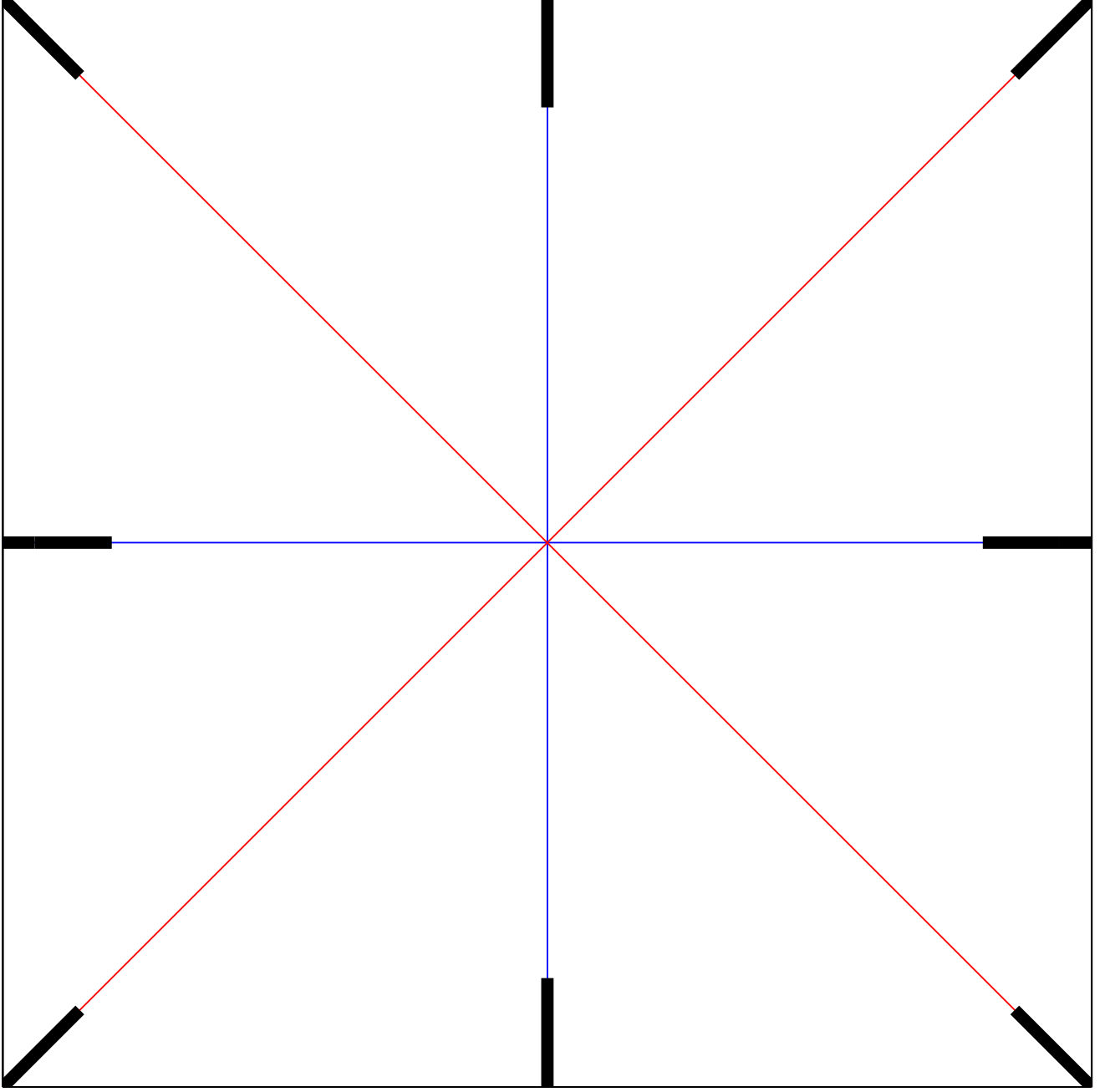


FIG. 5: Schematic figure of the laser arrangement. Black sticks indicate the lasers, red lines indicate 2λ -laser beams, and blue lines λ -laser beams.

potential is written as

$$\begin{aligned}
 V_{3D,1}(x, y, z) = & V_1 \cos^2 \left(\frac{2\pi x}{d} \right) + V_2 \cos^2 \left(\frac{2\pi y}{d} \right) + V_3 \cos^2 \left(\frac{2\pi z}{d} \right) + V_4 \cos^2 \left(\frac{\pi(x+y)}{d} + \theta_1 \right) \\
 & + V_5 \cos^2 \left(\frac{\pi(x-y)}{d} + \theta_2 \right) + V_6 \cos^2 \left(\frac{\pi(x+z)}{d} + \theta_3 \right) + V_7 \cos^2 \left(\frac{\pi(x-z)}{d} + \theta_4 \right). \quad (\text{A2})
 \end{aligned}$$

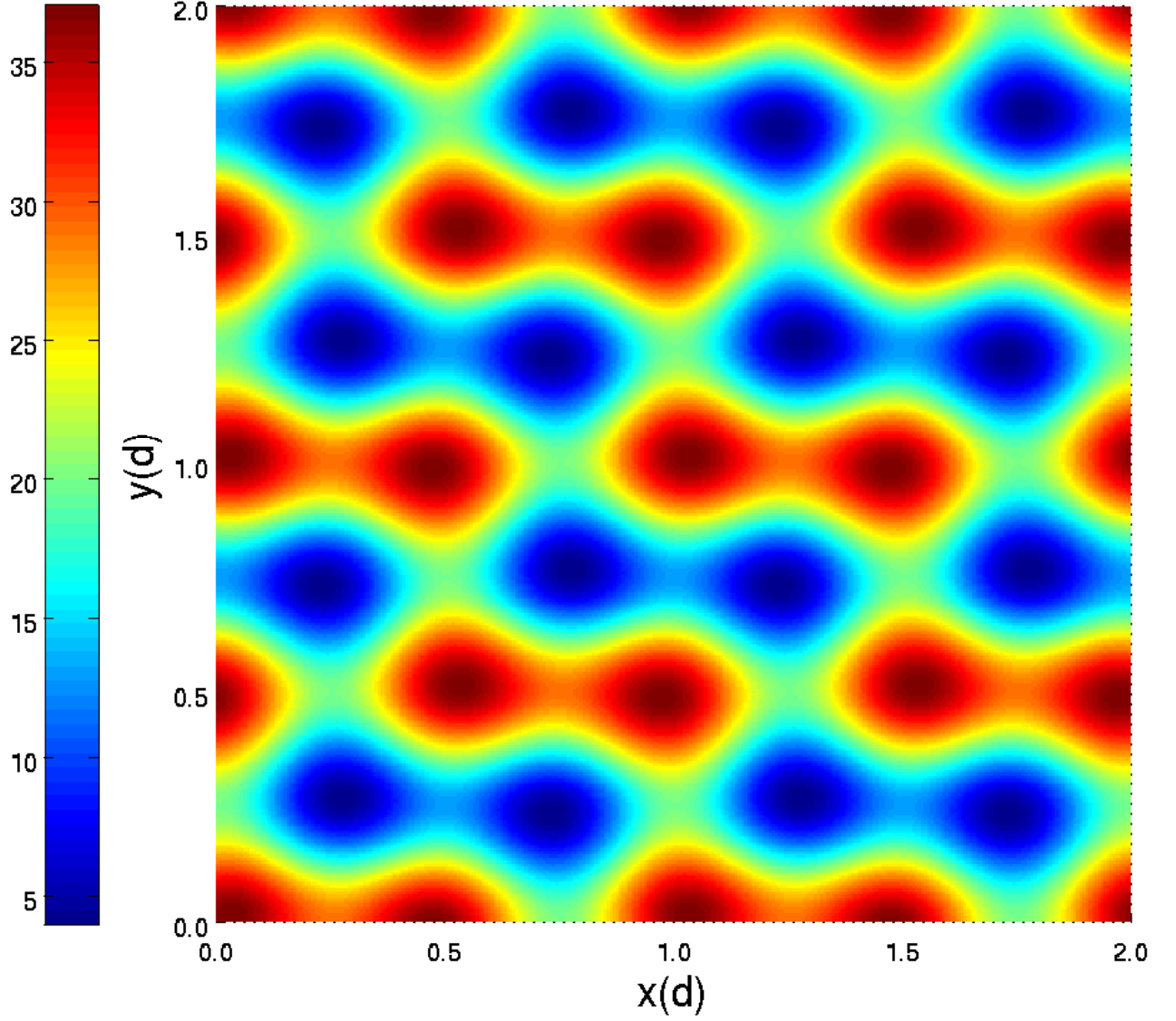


FIG. 6: 2D lattice potential with $V_1 = 12E_r$, $V_2 = 20E_r$, $V_3 = 8E_r$, $V_4 = 1E_r$, $\theta_1 = \pi/4$, and $\theta_2 = -\pi/4$, $E_r = \hbar^2\pi^2/(md^2)$ is the recoil energy. The color coding is such as: red=high values, blue=low values.

Alternatively, a more symmetric potential is given by

$$\begin{aligned}
 V_{3D,2}(x, y, z) = & V_1 \cos^2\left(\frac{2\pi x}{d}\right) + V_2 \cos^2\left(\frac{2\pi y}{d}\right) + V_3 \cos^2\left(\frac{2\pi z}{d}\right) + V_4 \cos^2\left(\frac{\pi(x+y)}{d} + \theta_1\right) \\
 & + V_5 \cos^2\left(\frac{\pi(x-y)}{d} + \theta_2\right) + V_6 \cos^2\left(\frac{\pi(x+z)}{d} + \theta_3\right) + V_7 \cos^2\left(\frac{\pi(x-z)}{d} + \theta_4\right) \\
 & + V_8 \cos^2\left(\frac{\pi(y+z)}{d} + \theta_5\right) + V_9 \cos^2\left(\frac{\pi(y-z)}{d} + \theta_6\right).
 \end{aligned} \tag{A3}$$

However, 18 lasers are needed to construct this potential.

Appendix B: Suprema and infima for the 3D lattice

If $J_{1,x} \neq J_{2,x}$ infima and suprema of $|V_{k_y, k_z}^+|$ and $|V_{k_y, k_z}^-|$ over the projected momentum space can be presented as functions of a_y, a_z, b_y, b_z . Without losing generality, we can assume $a_y, a_z, b_y, b_z \geq 0$. The supremum of $|V_{k_y, k_z}^+|$ is given by

$$\sup_{k_y, k_z} |V_{k_y, k_z}^+| = \begin{cases} a_y + a_z, & \text{if } a_y \geq b_y, a_z \geq b_z \\ b_y + b_z, & \text{if } a_y \leq b_y, a_z \leq b_z \\ \sqrt{\frac{(a_y^2 b_z^2 - a_z^2 b_y^2)(a_y^2 - b_y^2 + b_z^2 - a_z^2)}{(a_y^2 - b_y^2)(b_z^2 - a_z^2)}}, & \text{if } (a_y - b_y)(b_z - a_z) > 0, \text{ and } x_0, y_0 \in \mathbb{R}, \text{ and } |x_0|, |y_0| \leq 1, \\ \max(a_y + a_z, b_y + b_z), & \text{otherwise} \end{cases} \quad (\text{B1})$$

where

$$x_0 = \frac{b_y}{a_y^2 - b_y^2} \sqrt{\frac{-(a_y^4 a_z^2 + a_z^2 b_y^4 - a_y^2 [a_z^4 + b_z^4 + 2a_z^2(b_y^2 - b_z^2)])}{a_y^2 b_z^2 - a_z^2 b_y^2}}$$

$$y_0 = \frac{b_z}{b_z^2 - a_z^2} \sqrt{\frac{-(a_y^4 a_z^2 + a_z^2 b_y^4 - a_y^2 [a_z^4 + b_z^4 + 2a_z^2(b_y^2 - b_z^2)])}{a_y^2 b_z^2 - a_z^2 b_y^2}}.$$

The infimum of $|V_{k_y, k_z}^+|$ is given by

$$\inf_{k_y, k_z} |V_{k_y, k_z}^+| = \begin{cases} |b_y - b_z|, & \text{if } a_y \geq b_y, a_z \geq b_z \\ a_y \sqrt{1 - \frac{b_z^2}{b_y^2 - a_y^2}}, & \text{if } a_y < b_y, \frac{b_y b_z}{b_y^2 - a_y^2} \leq 1 \\ a_z \sqrt{1 - \frac{b_y^2}{b_z^2 - a_z^2}}, & \text{if } a_z < b_z, \frac{b_y b_z}{b_z^2 - a_z^2} \leq 1 \\ |b_y - b_z|, & \text{otherwise} \end{cases} \quad (\text{B2})$$

The supremum of $|V_{k_y, k_z}^-|$ is given by

$$\sup_{k_y, k_z} |V_{k_y, k_z}^-| = \begin{cases} \max(a_y, \sqrt{a_z^2 + b_y^2}), & \text{if } b_z = 0 \\ \max(a_z, \sqrt{a_y^2 + b_z^2}), & \text{if } b_y = 0 \\ b_y + b_z, & \text{if } a_y \leq b_y, a_z \leq b_z \\ a_y \sqrt{1 + \frac{b_z^2}{a_y^2 - b_y^2}}, & \text{if } a_y > b_y, \frac{b_y b_z}{a_y^2 - b_y^2} \leq 1 \text{ and } a_z \leq b_z \text{ or } \frac{b_y b_z}{a_z^2 - b_z^2} > 1 \\ a_z \sqrt{1 + \frac{b_y^2}{a_z^2 - b_z^2}}, & \text{if } a_z > b_z, \frac{b_y b_z}{a_z^2 - b_z^2} \leq 1 \text{ and } a_y \leq b_y \text{ or } \frac{b_y b_z}{a_y^2 - b_y^2} > 1 \\ \max\left(a_y \sqrt{1 + \frac{b_z^2}{a_y^2 - b_y^2}}, a_z \sqrt{1 + \frac{b_y^2}{a_z^2 - b_z^2}}\right), & \text{if } a_z > b_y, a_z > b_z \text{ and } \frac{b_y b_z}{a_y^2 - b_y^2} \leq 1, \frac{b_y b_z}{a_z^2 - b_z^2} \leq 1 \\ b_y + b_z, & \text{otherwise} \end{cases} \quad (\text{B3})$$

The infimum of $|V_{k_y, k_z}^-|$ is given by

$$\inf_{k_y, k_z} |V_{k_y, k_z}^-| = \begin{cases} 0, & \text{if } (a_y - a_z)(b_z - b_y) \geq 0 \\ \min(|a_y - a_z|, |b_y - b_z|), & \text{if } (a_y - a_z)(b_z - b_y) < 0 \text{ and } (a_y - b_y)(a_z - b_z) \leq 0 \\ \sqrt{\frac{(a_y^2 b_z^2 - a_z^2 b_y^2)(a_y^2 - b_y^2 + b_z^2 - a_z^2)}{(a_y^2 - b_y^2)(b_z^2 - a_z^2)}}, & \text{if } (a_y - b_y)(a_z - b_z) > 0, \text{ and } x_1, y_1 \in \mathbb{R}, \text{ and } |x_1|, |y_1| \leq 1 \\ \min(|a_y - a_z|, |b_y - b_z|), & \text{otherwise} \end{cases} \quad (\text{B4})$$

where

$$x_1 = \frac{b_y}{a_y^2 - b_y^2} \sqrt{\frac{-(a_y^4 a_z^2 + a_z^2 b_y^4 - a_y^2 [a_z^4 + b_z^4 + 2a_z^2(b_y^2 - b_z^2)])}{a_y^2 b_z^2 - a_z^2 b_y^2}}$$

$$y_1 = \frac{b_z}{a_z^2 - b_z^2} \sqrt{\frac{-(a_y^4 a_z^2 + a_z^2 b_y^4 - a_y^2 [a_z^4 + b_z^4 + 2a_z^2(b_y^2 - b_z^2)])}{a_y^2 b_z^2 - a_z^2 b_y^2}}.$$

References

-
- [1] B. A. Bernevig, T. L. Hughes, and S.-C. Zhang, *Science* **314**, 1757 (2006).
 - [2] L. Fu, C. L. Kane and E. J. Mele, *Phys. Rev. Lett.* **98**, 106803 (2007).
 - [3] M. König, S. Wiedmann, C. Brüne, A. Roth, H. Buhmann, L.W. Molenkamp, X.-L. Qi, and S.-C. Zhang, *Science* **318**, 766 (2007).
 - [4] D. Hsieh, D. Qian, L. Wray, Y. Xia, Y. Hor, R. J. Cava, and M. Z. Hasan, *Nature (London)* **452**, 970 (2008).
 - [5] M. Z. Hasan and C. L. Kane, *Rev. Mod. Phys.* **82**, 3045 (2010).
 - [6] X. Wan, A. M. Turner, A. Vishwanath, and S. Y. Savrasov, *Phys. Rev. B* **83**, 205101 (2011).
 - [7] A. A. Burkov and L. Balents, *Phys. Rev. Lett.* **107**, 127205 (2011).
 - [8] Z. K. Liu et al, *Science* **343**, 864 (2014).
 - [9] S. Borisenko, Q. Gibson, D. Evtushinsky, V. Zabolotnyy, B. Büchner, and R. J. Cava, *Phys. Rev. Lett.* **113**, 027603 (2014).
 - [10] S. Jeon, B. B. Zhou, A. Gyenis, B. E. Feldman, I. Kimchi, A. C. Potter, Q. D. Gibson, R. J. Cava, A. Vishwanath, and A. Yazdani, *Nat. Mat.* (2014), doi:10.1038/nmat4023.
 - [11] Y. Yamaji and M. Imada, *Phys. Rev. X* **4**, 021035 (2014).
 - [12] K. I. Petsas, A. B. Coates, and G. Grynberg, *Phys. Rev. A* **50**, 5173 (1994).
 - [13] C. Orzel, A. K. Tuchman, M. L. Fenselau, M. Yasuda, and M. A. Kasevich, *Science* **291**, 2386 (2001).
 - [14] J. K. Chin, D. E. Miller, Y. Liu, C. Stan, W. Setiawan, C. Sanner, K. Xu, and W. Ketterle, *Nature (London)* **443**, 961 (2006).
 - [15] P. Windpassinger and K. Sengstock, *Rep. Prog. Phys.* **76**, 086401 (2013).
 - [16] M. Bartenstein, A. Altmeyer, S. Riedl, R. Geursen, S. Jochim, C. Chin, J. Hecker Denschlag, R. Grimm, A. Simoni, C. J. Williams, and P. S. Julienne, *Phys. Rev. Lett.* **94**, 103201 (2005).
 - [17] T. D. Stanescu, V. Galitski, and S. Das Sarma, *Phys. Rev. A* **82**, 013608 (2010).
 - [18] K. Sun, W. V. Liu, A. Hemmerich, and S. Das Sarma, *Nat. Phys.* **8**, 67 (2012).
 - [19] Z. Lan, N. Goldman, A. Bermudez, W. Lu, and P. Öhberg, *Phys. Rev. B* **84**, 165115 (2011).
 - [20] M. Buchhold, D. Cocks, and W. Hofstetter, *Phys. Rev. A* **85**, 063614 (2012).
 - [21] F. Mei, S.-L. Zhu, Z.-M. Zhang, C. H. Oh, and N. Goldman, *Phys. Rev. A* **85**, 013638 (2012).
 - [22] C. J. Kennedy, G. A. Siviloglou, H. Miyake, W. C. Burton, and W. Ketterle, *Phys. Rev. Lett.* **111**, 225301 (2013).
 - [23] F. Grusdt, D. Abanin, and E. Demler, *Phys. Rev. A* **89**, 043621 (2014).
 - [24] M. Atala, M. Aidelsburger, J. T. Barreiro, D. Abanin, T. Kitagawa, E. Demler, and I. Bloch, *Nat. Phys.* **9**, 795 (2013).
 - [25] C. Weeks and M. Franz, *Phys. Rev. B* **85**, 041104 (2012).
 - [26] K. Sun, Z. Gu, H. Katsura, and S. Das Sarma, *Phys. Rev. Lett.* **106**, 236803 (2011).
 - [27] K. Nakada, M. Fujita, G. Dresselhaus and M. S. Dresselhaus, *Phys. Rev. B* **54**, 17954 (1996).
 - [28] T. Mizushima, M. Sato, and K. Machida, *Phys. Rev. Lett.* **109**, 165301 (2012).
 - [29] M. A. Silaev and G. E. Volovik, *Phys. Rev. B* **86**, 214511 (2012).
 - [30] A. P. Schnyder, C. Timm, and P. M. R. Brydon, *Phys. Rev. Lett.* **111**, 077001 (2013).
 - [31] P. M. R. Brydon, C. Timm, and A. P. Schnyder, *New J. Phys.* **15**, 045019 (2013).
 - [32] C. L. M. Wong, J. Liu, K. T. Law, and P. A. Lee, *Phys. Rev. B* **88**, 060504 (2013).
 - [33] J. D. Sau and S. Tewari, *Phys. Rev. B* **86**, 104509 (2012).
 - [34] A. Lau and C. Timm, arXiv:1305.1770 (2013).
 - [35] C.-R. Hu, *Phys. Rev. Lett.* **72**, 1526 (1994).
 - [36] Y. Tanaka and S. Kashiwaya, *Phys. Rev. Lett.* **74**, 3451 (1995).
 - [37] S. Kashiwaya and Y. Tanaka, *Rep. Prog. Phys.* **63**, 1641 (2000).
 - [38] G. E. Volovik, *JETP Lett.* **93**, 66 (2011).
 - [39] M. Sato, Y. Tanaka, K. Yada, T. Yokoyama, *Phys. Rev. B* **83**, 224511 (2011).
 - [40] Y. Tanaka, M. Sato, and N. Nagaosa, *J. Phys. Soc. Japan* **81**, 011013 (2012).
 - [41] T. T. Heikkilä, N. B. Kopnin, and G. E. Volovik, *JETP Lett.* **94**, 233 (2011); G. E. Volovik, *J. Supercond. Nov. Magn.* **26**, 2887 (2013).
 - [42] F. F. Assaad, M. Bercx, and M. Hohenadler, *Phys. Rev. X* **3**, 011015 (2013).
 - [43] B. Roy, F. F. Assaad, and I. F. Herbut, *Phys. Rev. X* **4**, 021042 (2014).
 - [44] T. Paananen and T. Dahm, *Phys. Rev. B* **87**, 195447 (2013).
 - [45] T. Paananen, H. Gerber, M. Götze, and T. Dahm, *New J. Phys.* **16** 033019 (2014).
 - [46] S. Ryu and Y. Hatsugai, *Phys. Rev. Lett.* **89**, 077002 (2002).
 - [47] M. Sato, *Phys. Rev. B* **73**, 214502 (2006).
 - [48] M. Fogelström, D. Rainer, and J.A. Sauls, *Phys. Rev. Lett.* **79**, 281 (1997).
 - [49] H. Walter, W. Prusseit, R. Semerad, H. Kinder, W. Assmann, H. Huber, H. Burkhardt, D. Rainer, and J. A. Sauls, *Phys. Rev. Lett.* **80**, 3598 (1998).
 - [50] M. Aprili, E. Badica, and L. H. Greene, *Phys. Rev. Lett.* **83**, 4630 (1999).
 - [51] R. Krupke and G. Deutscher, *Phys. Rev. Lett.* **83**, 4634 (1999).

- [52] B. Chesca, M. Seifried, T. Dahm, N. Schopohl, D. Koelle, R. Kleiner, A. Tsukada, Phys. Rev. B **71**, 104504 (2005).
- [53] B. Chesca, D. Dönitz, T. Dahm, R. P. Huebener, D. Koelle, R. Kleiner, Ariando, H.-J. H. Smilde, H. Hilgenkamp, Phys. Rev. B **73**, 014529 (2006).
- [54] C. Iniotakis, T. Dahm, and N. Schopohl, Phys. Rev. Lett. **100**, 037002 (2008).
- [55] S. Graser, C. Iniotakis, T. Dahm, and N. Schopohl, Phys. Rev. Lett. **93**, 247001 (2004).
- [56] A. Zare, T. Dahm, and N. Schopohl, Phys. Rev. Lett. **104**, 237001 (2010); A. Zare, A. Markowsky, T. Dahm, and N. Schopohl, Phys. Rev. B **78**, 104524 (2008).
- [57] A. P. Zhuravel, B. G. Ghamsari, C. Kurter, P. Jung, S. Remillard, J. Abrahams, A. V. Lukashenko, A. V. Ustinov, and S. M. Anlage, Phys. Rev. Lett. **110**, 087002 (2013).
- [58] N. B. Kopnin, JETP Lett. **94**, 81 (2011).
- [59] N. B. Kopnin, M. Ijäs, A. Harju, T. T. Heikkilä, Phys. Rev. B **87**, 140503(R) (2013).
- [60] S. Matsuura, P.-Y. Chang, A. P. Schnyder, and S. Ryu, New J. Phys. **15**, 065001 (2013).
- [61] K. Osterloh, M. Baig, L. Santos, P. Zoller, and M. Lewenstein, Phys. Rev. Lett. **95**, 010403 (2005)..
- [62] J. Ruseckas, G. Juzeliunas, P. Öhberg, and M. Fleischhauer, Phys. Rev. Lett. **95**, 010404 (2005).
- [63] S. Ryu, A. P. Schnyder, A. Furusaki and A. Ludwig, New J. Phys. **12**, 065010 (2010).
- [64] A. P. Schnyder, S. Ryu, A. Furusaki and A.W.W. Ludwig, Phys. Rev. B **78**, 195125 (2008).
- [65] A. P. Schnyder and S. Ryu, Phys. Rev. B **84**, 060504(R) (2011); P. M. R. Brydon, A.P. Schnyder, and C. Timm, Phys. Rev. B **84**, 020501(R) (2011); A.P. Schnyder, P. M. R. Brydon, and C. Timm, Phys. Rev. B **85**, 024522 (2012).